nature physics

ARTICLES

https://doi.org/10.1038/s41567-022-01544-9

Simulation of open quantum systems by automated compression of arbitrary environments

Moritz Cygorek[1]✉, Michael Cosacchi[2], Alexei Vagov[2,3], Vollrath Martin Axt[2], Brendon W. Lovett[4], Jonathan Keeling[4] and Erik M. Gauger[1]✉

Studies of the dynamics of open quantum systems are limited by the large Hilbert space of typical environments, which is too large to be treated exactly. In some cases, approximate descriptions of the system are possible, for example, when the environment has a short memory time or only interacts weakly with the system. Accurate numerical methods exist, but these are typically restricted to baths with Gaussian correlations, such as non-interacting bosons. Here we present a method for simulating open quantum systems with arbitrary environments that consist of a set of independent degrees of freedom. Our approach automatically reduces the large number of environmental degrees of freedom to those which are most relevant. Specifically, we show how the process tensor describing the effect of the environment can be iteratively constructed and compressed using matrix product state techniques. We demonstrate the power of this method by applying it to a range of open quantum systems, including bosonic, fermionic and spin environments. The versatility and efficiency of our automated compression of environments method provides a practical general-purpose tool for open quantum systems.

An inevitable property of quantum technologies is that quantum devices interact with their environment[1]. This interaction gives rise to dephasing and dissipation, but—if understood—it can be exploited, for example, in environment-assisted quantum transport[2–4] or even quantum information processing[5,6]. Because of the exponential growth of the Hilbert space dimension, as well as the large number of environmental degrees of freedom, the direct solution of Schrödinger's equation for the system and environment is usually infeasible. As such, one requires practical methods that allow the simulation of the system dynamics and accounting for effects of the environment[1,7–9].

Among such approaches, those most frequently used rely on the Born and Markov approximations, which enable one to derive time-local equations of motion for the reduced system density matrix[1,10]. The Born approximation implies that the environment does not substantially change with time—that is, system–environment correlations are weak and transient. Although valid for weakly coupled open quantum systems, other environments lead to strong system–environment correlations[11]. The Markov approximation depends on the memory time of the environment being short compared with the time evolution of the system. This fails if the spectral density is highly structured or if there is a long memory time[12]. Given these widespread limitations, approaches beyond the Born–Markov approximation are clearly necessary.

Numerically convergent methods, where tuning the convergence parameters allows one to systematically trade off precision against computation time, do exist for some non-Markovian problems, for example, those where the environments have Gaussian correlations, such as non-interacting bosonic modes. Such methods include hierarchical equations of motion[13,14], chain mapping through orthogonal polynomials[15–17] or the Feynman–Vernon real-time path integral formalism[18]. In particular, the iterative form of the path integral[19–21] and its reformulation with matrix product operators (MPOs)[22] have been successfully used, for example, to simulate phonon effects on spectra[23,24], to devise robust and high-fidelity protocols for the emission of non-classical light[25–27] and to model concrete experiments on optically driven quantum dots (QDs)[28–30]. Such approaches have been extended to systems with multiple environments[31], multilevel systems[21] and special types of non-Gaussian bath such as quadratic coupling to bosons or fermions[32]. Some methods for general environments do exist, such as correlation expansion[33], but it is complicated to derive these equations at higher expansion order. Likewise, although a stochastic formulation of the equations of motion is formally possible for baths with arbitrary statistics[34], the prerequisite of operating on higher-order multitime correlation functions poses challenges for practical applications, except for special cases[35]. As such, a challenge remains: to provide general and efficient numerically convergent methods that can also model non-Gaussian non-Markovian environments.

Here we provide such a method, which can be used to simulate open quantum systems coupled to arbitrary environments (Fig. 1a). We demonstrate its practical application with a variety of forms of environments: bosonic, fermionic and spins. Because the derivation is general, the same code can be used to simulate the dynamics of a large variety of different physical systems. At the core of our automated compression of environments (ACE) method is the explicit microscopic construction of the process tensor (PT)[36,37]—an object originally conceived as a way to conceptualize correlations for a general non-Markovian environment—and a route to efficiently compress this object using MPO techniques[38,39]. Specifically, we provide a general and efficient algorithm to directly construct an MPO representation of the PT, corresponding to an automated projection of the environment onto its most relevant degrees of freedom.

Results

ACE. The working principle of ACE is to efficiently represent the environment by concentrating on its most relevant degrees of freedom (Fig. 1a). These are automatically selected using MPO

[1]SUPA, Institute of Photonics and Quantum Sciences, Heriot-Watt University, Edinburgh, UK. [2]Theoretische Physik III, Universität Bayreuth, Bayreuth, Germany. [3]HSE University, Moscow, Russia. [4]SUPA, School of Physics and Astronomy, University of St Andrews, St Andrews, UK. ✉e-mail: m.cygorek@hw.ac.uk; e.gauger@hw.ac.uk

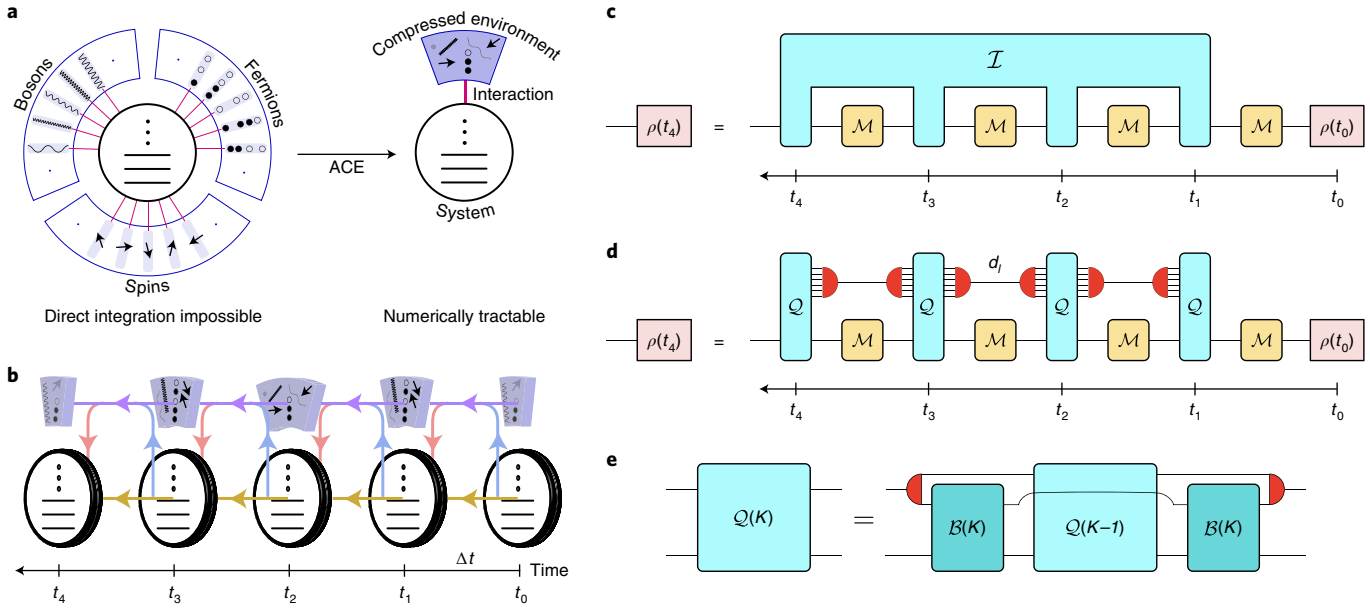

Fig. 1 | Depiction of the ACE approach. a, Identification of an efficient representation is fully automatic and does not rely on any a priori approximations or assumptions. **b**, Time evolution of the system plus its compressed environment proceeds in discrete time steps. The information flow is indicated by coloured arrows. **c**, Formally, the general propagation of a quantum system can be expressed with a PT $\mathcal{I}$. **d**, Propagation with a PT in its MPO form: this corresponds to the schematic of the situation shown in **b**. **e**, Combination of the influence of environment mode K with the PT containing the influences of modes $1, 2, \ldots, K-1$. The red semicircles indicate the effects of MPO compression (schematic in **a** and **b**).

compression techniques and may differ from one time step to another. This procedure guarantees fully capturing the non-Markovian information flow from past time steps to later time steps via the environment (Fig. 1b). We now summarize the ACE method introduced in this paper; further details are provided in Methods. Our goal is to obtain the reduced system density matrix $\rho_{\nu\mu}(t)$ at time t, accounting for coupling to a given environment. We discretize the time axis on a grid with equal time steps Δt where the l-th time step starts at $t_l = l\Delta t$ (Fig. 1b–d); then, for a single time step, the time evolution operator $U(\Delta t) = \mathrm{e}^{-\frac{\mathrm{i}}{\hbar}H\Delta t}$ of the total system can be factorized using the Trotter expansion $U(\Delta t) = \mathrm{e}^{-\frac{\mathrm{i}}{\hbar}H_\mathrm{E}\Delta t}\mathrm{e}^{-\frac{\mathrm{i}}{\hbar}H_\mathrm{S}\Delta t} + \mathcal{O}(\Delta t^2)$, where the total Hamiltonian $H = H_\mathrm{S} + H_\mathrm{E}$ is decomposed into the system Hamiltonian H_S and environment Hamiltonian H_E including the system–environment coupling. Here, $\hbar$ is Planck's constant and $\mathcal{O}(\Delta t^2)$ denotes an error of second order in Δt. Inserting a complete set of basis states for the system and the environment and tracing out the environment, the reduced system density matrix at time t_n can be written as

$$\rho_{\alpha_n} = \sum_{\substack{\alpha_{n-1}\ldots\alpha_0 \\ \tilde{\alpha}_n\ldots\tilde{\alpha}_1}} \mathcal{I}^{(\alpha_n\tilde{\alpha}_n)\ldots(\alpha_1\tilde{\alpha}_1)} \left(\prod_{l=1}^{n} \mathcal{M}^{\tilde{\alpha}_l\alpha_{l-1}}\right) \rho_{\alpha_0}, \tag{1}$$

where we have defined $\alpha = (\nu, \mu)$ to combine two Hilbert space indices into a single Liouville space index. A visual representation of equation (1) is depicted in Fig. 1c. Here $\mathcal{M}$ describes the free propagation of the system. This can be time dependent, and can additionally include effects of Markovian baths. The effects of the general non-Markovian non-Gaussian environment are captured in quantity $\mathcal{I}$, which is the PT here. This object slightly differs from the original definition of the PT[37], where we have separated out the initial state and free-system evolution. When $\mathcal{I}$ is non-zero only for diagonal couplings $\alpha_l = \tilde{\alpha}_l$, this object becomes equivalent to the Feynman–Vernon influence functional[18]. The PT can, thus, be considered as a generalization of this influence functional to the case of non-diagonal couplings. From the explicit expression for the PT, we find that it automatically has the form of an MPO:

$$\mathcal{I}^{(\alpha_n,\tilde{\alpha}_n)(\alpha_{n-1},\tilde{\alpha}_{n-1})\ldots(\alpha_1,\tilde{\alpha}_1)} = \sum_{d_{n-1}\ldots d_1} \mathcal{Q}_{1d_{n-1}}^{(\alpha_n,\tilde{\alpha}_n)} \mathcal{Q}_{d_{n-1}d_{n-2}}^{(\alpha_{n-1},\tilde{\alpha}_{n-1})} \ldots \mathcal{Q}_{d_1 1}^{(\alpha_1,\tilde{\alpha}_1)}. \tag{2}$$

Here the dimension of the inner indices d_l is very large, corresponding to a complete basis of environment states in Liouville space. This large dimension precludes the direct application of equations (1) and (2) for typical environments. However, the MPO form of the PT means that it is, in principle, amenable to standard MPO compression, based on singular-value decomposition (SVD), as described in Methods[38,39]. Such compression physically corresponds to reducing the environment to its most relevant degrees of freedom, which—as theoretical consideration of PTs suggest[40]—may be few in number.

The key challenge is, thus, to find an efficient way to calculate the compressed form of the PT MPO, without first constructing the uncompressed PT. This can be achieved through the ACE approach, for any problem with an environment that can be decomposed into N_E different non-interacting degrees of freedom:

$$H = H_\mathrm{S} + \sum_{k=1}^{N_\mathrm{E}} H_\mathrm{E}^k. \tag{3}$$

The label k can describe both the different degrees of freedom within a bath (for example, different spins or photon modes defined by their wave vector $\mathbf{q}$), but can also enumerate multiple environments coupled to the same system. In all these cases, the PT can be iteratively constructed by successively adding the contribution of the degree of freedom of each bath. The process of combining the influence of the Kth degree of freedom, $\mathcal{B}[K]$, with an existing PT MPO $Q(K-1)$ is shown in Fig. 1e. If the resulting MPOs are compressed after each step (Fig. 1e, red semicircles), the inner dimension remains manageable and exact diagonalization can be used for the SVD. This is described in more detail in Methods.

Once the compressed PT in the MPO representation is obtained, it can be substituted into equation (1). The calculation of the reduced

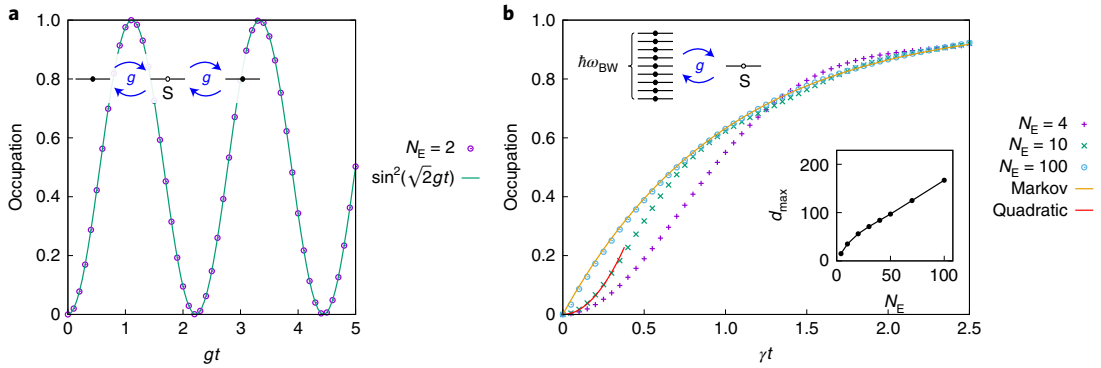

Fig. 2 | Resonant-level model application of ACE, spanning small to infinite bath memory time. a, Dynamics of the occupations of a single localized quantum state (S) coupled to two resonant environment modes. **b**, Dynamics of a quantum state coupled to a quasi-continuum of modes. ACE simulations (points) are shown together with analytical solutions (lines). The analytical result in the Markov limit corresponds to an exponential transfer with the rate obtained from the Fermi's golden rule. The result of a quadratic Taylor expansion around $t=0$ is depicted for the case of $N_E=10$. The top-left insets depict the respective physical situations. The bottom-right inset shows the maximum inner dimension d_{max} of the PT MPO as a function of the number of environment states N_E for a constant density of states.

system density matrix then amounts to the contraction of a network of the form shown in Fig. 1d. If the PT MPO has a sufficiently small inner dimension, this contraction is straightforward. Because this algorithm can be applied, in principle, to arbitrary environments simply by specifying the respective environment Hamiltonians H_E^k, ACE allows the investigations of a huge variety of different open quantum systems. We next show how this method works in practice for a few paradigmatic example problems.

Resonant-level model. As the first test of ACE, we consider the archetypal problem of electron transport between a single localized electron state and other nearby environment states, described by the resonant-level model. The kth environment state is described by

$$H_E^k = \hbar\omega_k c_k^\dagger c_k + \hbar g_k (c_k^\dagger c_S + c_S^\dagger c_k), \tag{4}$$

where $c_S^\dagger(c_S)$ and $c_k^\dagger(c_k)$ create (destroy) a fermion in the localized system state and the kth environment state, respectively; $\hbar\omega_k$ is the energy of the kth environment state with respect to the system state; and g_k is the coupling constant, which we assume to be independent of k, and $g_k=g$. The free-system Hamiltonian is $H_S=0$. The Hamiltonian in equation (4) shows a distinct behaviour depending on the number of environment modes: coherent oscillations for few modes and irreversible decay for a broad continuum of modes. In the following, we show that ACE can automatically capture both these limits and interpolate between them.

For a few environment modes, the dynamics is described by coherent oscillations at the eigenfrequencies of the coupled system and environment. Here we consider the situation depicted in Fig. 2a, inset, where a single initially empty site is connected to two sites at the same energy $\omega_k=0$, which are initially occupied. In this scenario, the time-dependent many-body state of the total system is

$$|\Psi(t)\rangle = \left[\cos(\sqrt{2}gt)\frac{c_1^\dagger + c_2^\dagger}{\sqrt{2}} - \mathrm{i}\sin(\sqrt{2}gt)c_S^\dagger\right]\frac{c_1^\dagger - c_2^\dagger}{\sqrt{2}}|0\rangle\,. \tag{5}$$

In Fig. 2a, we compare the occupation $n_S = \sin^2(\sqrt{2}gt)$ with the results of the ACE simulations for convergence parameters $\Delta t=0.01g$ and $\epsilon=10^{-7}$ (Methods). We see that the results match perfectly. Since the oscillations are undamped, the memory time of the environment is infinite. Furthermore, when $n_S=\frac{1}{2}$, equation (5) describes a state with the maximum entanglement between the system and the environment. This demonstrates that ACE can account for infinite memory times as well as strong system–environment correlations.

Different behaviours occur for a quasi-continuum of environment states, for example, metallic leads coupled to a QD[41] (Fig. 2b, top-left inset). The oscillatory contributions of the different modes interfere destructively, suppressing oscillations. When the continuum is broad enough, there is a short memory time and weak system–bath correlations; therefore, the situation is well described by Markovian master equations. These predict charge transfer to the localized state at a rate $\gamma=2\pi\hbar g^2 D$, where $D=(N_E-1)/(\hbar\omega_{BW})$ is the density of states and $\hbar\omega_{BW}$ is the bandwidth. Figure 2b shows the corresponding dynamics for different numbers of environment modes N_E with a fixed density of states $D=1/(\hbar\gamma)$. As the number of environment modes (and therefore the bandwidth) increases, the simulations approach the Markovian analytical result $(1-\exp(-\gamma t))$. For intermediate $N_E=10$, the finite bandwidth introduces a finite memory time of $\sim 1/\omega_{BW}$. To check the validity of the ACE results in this more complicated cross-over regime, we also plot the analytical short-time Taylor expansion $n_S \approx \gamma\omega_{BW}t^2/(2\pi)$ for the case of $N_E=10$.

Figure 2b, inset, shows the maximum inner dimension d_{max} of the PT MPO as a function of the number of modes N_E. We see this scales linearly with the number of modes, indicating a very efficient reduction, compared with the exponential scaling of the dimension of the full-environment Liouville space of up to $4^{100}\approx 1.6\times10^{60}$ for $N_E=100$. A more detailed analysis of numerical convergence is given in Supplementary Section 2. This simple example demonstrates that ACE is able to reproduce analytical results in all the regimes: from infinite memories to Markovian environments and from strong to weak system–environment correlations.

Simultaneous coupling of QDs to phonons and electromagnetic-field modes. Our second example involves a system simultaneously coupled to two structured baths, as exemplified by a semiconductor QD, coupled both to acoustic phonons and an electromagnetic environment. The acoustic phonon modes couple via a pure-dephasing interaction:

$$H_{ph}^{\mathbf{q}} = \hbar\omega_{\mathbf{q}} b_{\mathbf{q}}^\dagger b_{\mathbf{q}} + \hbar\gamma_{\mathbf{q}}\left(b_{\mathbf{q}}^\dagger + b_{\mathbf{q}}\right)|e\rangle\langle e|\,, \tag{6}$$

where $b_{\mathbf{q}}^\dagger$ ($b_{\mathbf{q}}$) creates (annihilates) a phonon with wave vector $\mathbf{q}$. Throughout this article, $|g\rangle$ and $|e\rangle$ denote the ground and excited states of the QD, respectively. If this were the only interaction, its

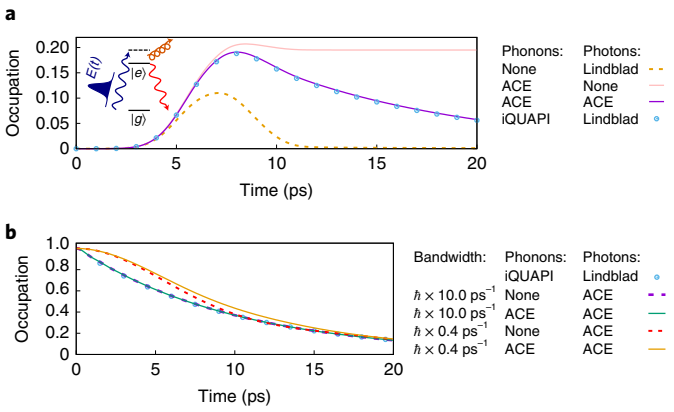

Fig. 3 | Dynamics of QDs embedded in (non-additive) photon and phonon environments. a, Dynamics of the exciton occupation for phonon-assisted off-resonant excitation of a QD driven by a Gaussian laser pulse and subject to radiative decay according to different theoretical approaches: the QD–phonon interaction may be disregarded (none) or treated within ACE or iQUAPI. The coupling between the QD and photonic modes may be disregarded (none), included explicitly in ACE via its Hamiltonian, or replaced by a Lindblad term for radiative decay. **b**, Radiative decay of an initially occupied exciton state with and without interactions with phonons for model photon densities of states with different bandwidths $\hbar\omega_{\mathrm{BW}}$.

linear and diagonal structures would mean it could be treated within the iterative quasi-adiabatic path integral (iQUAPI) method[19,21,23]. Below, we will compare the results of ACE with those of iQUAPI.

In addition to the bath of phonons, QDs also couple to the continuum of electromagnetic modes, which are responsible for radiative decay. Here the interaction with photon mode k takes the following Jaynes–Cummings form:

$$H_{\mathrm{JC}}^{k} = \hbar\omega_k a_k^{\dagger} a_k + \hbar g_k \left(a_k^{\dagger} \left|g\right\rangle \left\langle e\right| + a_k \left|e\right\rangle \left\langle g\right| \right), \tag{7}$$

where $a_k^{\dagger}$ (a_k) is the bosonic creation (annihilation) operator for a photon in mode k.

There are several ways of including both baths in the simulations: first, for unstructured (that is, Markovian) photon environments, the Born–Markov approximation holds; therefore, we can account for the radiative decay as the Lindblad term $\kappa\mathcal{L}\left[\left|g\right\rangle\left\langle e\right|, \rho\right]$, where

$$\begin{aligned} &\mathcal{L}\left[\left|g\right\rangle\left\langle e\right|, \rho\right] \\ &\equiv \left|g\right\rangle\left\langle e\right| \rho \left|e\right\rangle\left\langle g\right| - \tfrac{1}{2}\left(\left|e\right\rangle\left\langle e\right| \rho + \rho \left|e\right\rangle\left\langle e\right|\right). \end{aligned} \tag{8}$$

In both ACE and iQUAPI[42], such Markovian dissipation can be included into the free-system Liouville propagator $\mathcal{M}$. Due to the flexibility of ACE, we can also microscopically describe the radiative decay by including both phonon and electromagnetic environments in the PT. This has the advantage that it automatically captures possible non-additive effects of the simultaneous coupling to multiple baths[43–46], as well as allows one to extend to structured electromagnetic environments.

In Fig. 3a, we show how the occupation of a QD responds to off-resonant excitation by a Gaussian laser pulse. This drive corresponds to the following time-dependent Hamiltonian in the rotating frame of the laser:

$$H_{\mathrm{S}} = -\hbar\delta \left|e\right\rangle\left\langle e\right| + \frac{\hbar}{2}\Omega(t)\left(\left|e\right\rangle\left\langle g\right| + \left|g\right\rangle\left\langle e\right|\right), \tag{9}$$

where δ is the laser detuning and $\Omega(t)$ is a Gaussian envelope centred at $t_0 = 7$ ps with pulse duration $\tau_{\mathrm{FWHM}} = 5$ ps. The QD simultaneously interacts with the phonon and photon baths, which are treated within different theoretical approaches. In this figure, we assume a flat electromagnetic environment; therefore, all the approaches should work equally well. The simulation parameters describe a GaAs QD[47] and are summarized in Methods.

In the absence of QD–phonon interactions, the exciton is only transiently occupied during the pulse, as absorption is suppressed by the detuning of the laser from the exciton energy. Including phonons within ACE but disregarding radiative decay entirely results in a non-zero stationary-exciton occupation, as the detuning may be bridged by phonon emission. Including both phonons and photons, one sees absorption followed by radiative decay. Identical results are found for this case for ACE (microscopically treating the electromagnetic environment) as well as for iQUAPI with photon decay $\kappa\mathcal{L}\left[\left|g\right\rangle\left\langle e\right|, \rho\right]$. As such, we both further confirm the capabilities of ACE, and see that—as may be anticipated—for an unstructured photon environment, no cross-action between the coupling to photon and phonon baths can be identified.

As already noted, ACE is also able to treat situations with non-additive environments, as is relevant for structured photonic environments like waveguides or microcavities[48,49]. Figure 3b shows the decay of an initially occupied exciton state (with $H_{\mathrm{S}} = 0$) where, in addition to the non-Markovian phonon bath, we use a photon bath with a finite bandwidth $\hbar\omega_{\mathrm{BW}}$. For large bandwidths, no cross-interaction between the couplings to the two baths is found (and therefore the results again match iQUAPI with Lindbladian photon loss). For small bandwidths $\omega_{\mathrm{BW}} = 0.4\,\mathrm{ps}^{-1}$, the photon environment yields a memory time $\tau \approx 1/\omega_{\mathrm{BW}}$ of the same order of magnitude as the phonon environment. As a result, the two baths couple non-additively, as evident from the fact that the coupling to phonons substantially influences the decay of excitations into the electromagnetic modes.

Spin dynamics. Our third example concerns the spin dynamics in the presence of a spin environment[50,51]. Besides demonstrating the applicability of ACE to non-Gaussian spin environments, this example also identifies the limits on efficient environment compression. We consider a central spin coupled to a bath of environment spins by a Heisenberg interaction

$$H_{\mathrm{E}}^{k} = \frac{J_k}{\hbar^2}\,\mathbf{S}\cdot\mathbf{s}_k, \tag{10}$$

where $\mathbf{S}$ and $\mathbf{s}_k$ are the spin-$\frac{1}{2}$ operators of the central spin and kth environment spin, respectively (Fig. 4, inset). In the following, we choose the coupling constants $J_k = J/N$, where N is the number of environment spins and J defines the energy scale of the coupling. We set $H_{\mathrm{S}} = 0$ and initially prepare the system spin in the state with maximum $\langle S_x\rangle$. We then explore how the initial degree of polarization of the environment affects the system dynamics, as well as the ability to efficiently compress the environment.

First, we focus on the situation where the environment spins are completely polarized along the z axis. The respective dynamics of $\langle S_x\rangle$ is depicted in Fig. 4a for $N = 10$, 100 and 1,000 and for convergence parameters $\Delta t = 0.01\hbar/J$ and $\epsilon = 10^{-10}$. The Heisenberg coupling leads to a coherent precession of the system and environment spins about each other. In the limit $N \to \infty$, there is no back-action on the environment; therefore, the environment remains in its initial state. The dynamics is then equivalent to a precession about a constant effective magnetic field, for which $\langle S_x\rangle = (\hbar/2)\cos(tJ/2\hbar)$. We see the ACE simulations for $N = 1{,}000$ approach this limit. It is noteworthy that for all N, the inner dimension of the PT MPO remains 4, corresponding to the Liouville space dimension of a single spin $\frac{1}{2}$. This is because all the environment spins behave identically; therefore, the environment can be replaced by a single effective spin.

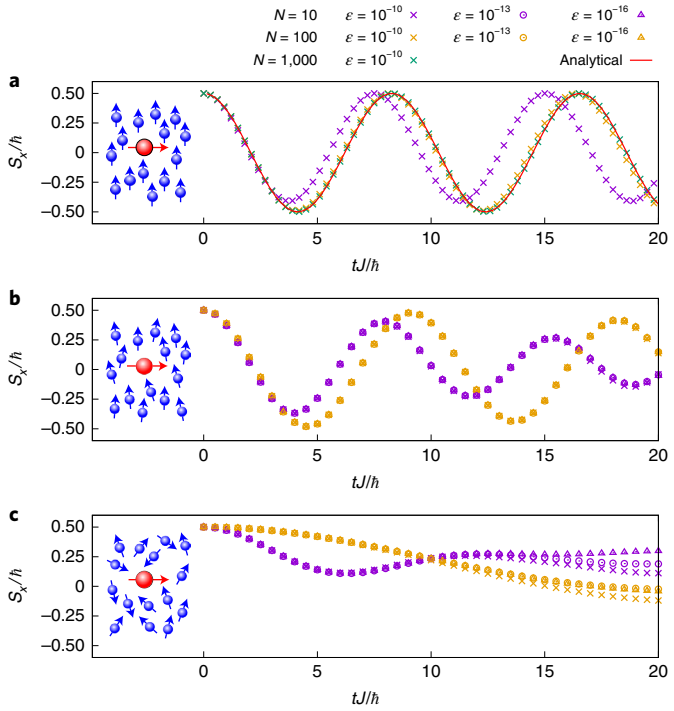

Fig. 4 | Central spin model for different degrees of spin bath polarization. **a**–**c**, Dynamics of a central spin (red) initially prepared along the *x* axis in a bath of *N* spins (blue), as shown in the insets. The *x* component of a central spin is shown for situations where the bath spins are fully polarized (**a**), partially polarized (**b**) or unpolarized (**c**). The number of environment spins *N* is varied, keeping the sum of the couplings $\sum_k J_k = J$ as constant. The colours correspond to different numbers of environment spins *N*, whereas the point types correspond to different values of the MPO compression threshold ϵ.

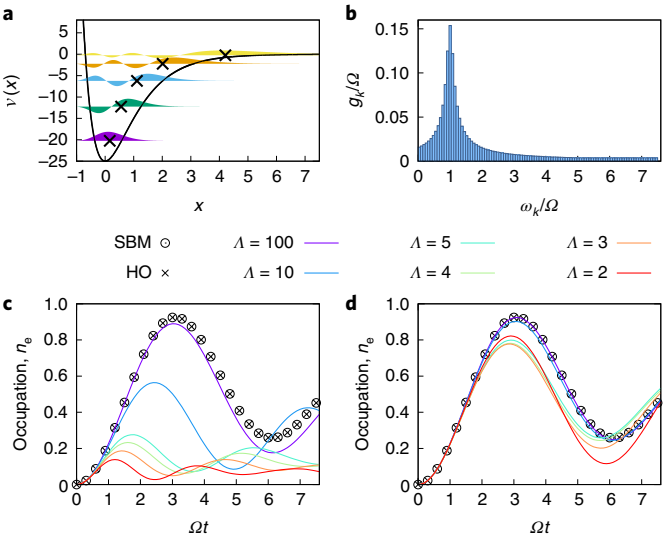

Fig. 5 | Two-level system coupled to a bath of anharmonic modes. **a**, Morse potential (equation (11)) with parameter $\Lambda = 5$ and its bound eigenstates obtained numerically. The crosses mark the average position $\langle i|\,\hat{x}\,|i\rangle$ for each eigenstate. **b**, Coupling coefficients g_k corresponding to a Lorentzian spectral density of environment modes. **c**, ACE simulations with $M = \min\{5, \Lambda\}$ environment levels for the spin-boson model (SBM), harmonic oscillator (HO) modes obtained by the finite differences method and finite differences solutions of the Morse potential for different Λ values. **d**, Analogous calculations to **c** but where energy shifts due to non-zero $\langle i|\,\hat{x}\,|i\rangle$ have been subtracted.

We next explore the limitations of compression of the environment by considering randomized initial conditions for the environment spins. In Fig. 4b,c, we present the ACE simulations with $N = 10$ and $N = 100$ environment spins for different values of the MPO truncation threshold ϵ. In Fig. 4b, the bath is partially polarized: we randomly select pure spin states from an isotropic distribution and filter these with the rejection probability $1 - \exp\left[b\left(s_k^z/\hbar - \frac{1}{2}\right)\right]$. Here $b = (g_s\mu_B B)/(k_B T)$ is a Boltzmann factor with gyromagnetic ratio g_s, Bohr magneton μ_B, magnetic field B, and Boltzmann constant k_B, taken as $b = 20$ (Fig. 4b). In Fig. 4c, we instead use a uniform distribution (that is, $b = 0$). In both cases, a dephasing of the central spin is visible. However, for the unpolarized case, the spin dynamics for different ϵ values start to diverge at long times. The slow convergence with ϵ in this situation is a consequence of the intrinsic incompressibility of the environment degrees of freedom. That is, because each environment spin reacts differently to the system spin, the joint PT cannot be efficiently compressed. Furthermore, environment spins can become correlated via an effective interaction mediated by the system; without an external magnetic field, the environment states are highly degenerate. Consequently, there is no clear physical constraint on the accessible-environment Hilbert space. In the partially polarized case, the environment can be compressed more efficiently; therefore, the ACE simulations show better convergence.

Anharmonic environments. Although a multitude of numerically convergent methods exist to describe Gaussian environments like a bath of harmonic oscillators, few are available that can address anharmonic modes, which render the environment non-Gaussian. These typically work by explicitly propagating the joint system and environment state using an appropriately chosen representation[52]. ACE implicitly identifies such a representation automatically in the form of compressed inner bonds of the PT.

Anharmonicities are found in practice, for example, in the vibrational modes of molecules with a finite number of bound vibrational states, commonly modelled by a Morse potential[53]

$$v(x) = \Lambda^2\left(\mathrm{e}^{-2x} - 2\mathrm{e}^{-x}\right), \tag{11}$$

where Λ controls the depth of the potential as well as the number of bound states. Here we use the Morse potential as a demonstration of simulating the environment modes with arbitrary potentials $v(x)$.

As described in more detail in Supplementary Section 4, we first use a finite differences method to numerically find the eigenstates of a single uncoupled environment mode, before introducing coupling to the system. For example, the bound eigenstates of the Morse potential for $\Lambda = 5$ are depicted in Fig. 5a. Keeping only the M lowest-energy eigenstates and choosing a system–environment coupling proportional to the environment position operator, we find that for environment mode k,

$$H_{\mathrm{E}}^k = \sum_{j=0}^{M-1} \hbar\omega_k \tilde{E}_j \sigma_{jj}^k + \hbar g_k \sum_{i,j=0}^{M-1} \sqrt{2}\,\langle i|\,\tilde{x}\,|j\rangle\,\sigma_{ij}^k\,|e\rangle\langle e|\,, \tag{12}$$

where $\tilde{E}_j$ and $\langle i|\,\tilde{x}\,|j\rangle$ are scaled so that the spin-boson model Hamiltonian is recovered when $v(x)$ is the harmonic oscillator potential.

ACE simulations are performed for $H_S = \frac{\hbar}{2}\Omega\left(|e\rangle\langle g| + |g\rangle\langle e|\right)$, describing a continuously driven system performing Rabi oscillations damped by the anharmonic environment. We choose a set of ω_k and g_k values that correspond to a Lorentzian spectral density

(Fig. 5b); Supplementary Section 4 describes the other parameters. The resulting excited-state occupations n_e are shown in Fig. 5c.

As a validity check, we first apply the above method to a harmonic potential, and exactly recover the dynamics of the spin-boson model. On moving to Morse potential environments, we find substantial differences, especially for small Λ. Much of the difference is due to the asymmetry of the Morse potential, leading to an average position $\langle i|\tilde{x}|i\rangle$ that increases for higher-excited states (Fig. 5a, crosses). This enters in H_E via the system–environment coupling and results in an energy shift of the $|e\rangle$ system state. To better identify the intrinsic effects of anharmonicity, Fig. 5d shows ACE results where this shift has been subtracted. For small Λ, the effects of anharmonicity of the Morse potential are evident, whereas for large Λ, the anharmonicity becomes negligible and the result of the Gaussian simulations is recovered.

Discussion

We have presented a numerically convergent, efficient and versatile method, namely, ACE, which makes it possible to simulate the dynamics of N-level quantum systems coupled to arbitrary environments directly from the microscopic system–environment coupling Hamiltonian. We have illustrated the power of this method with examples of electron transport, the simultaneous interaction of a QD with phonon and photon modes, spin dynamics and anharmonic environments. In Supplementary Section 5, we provide an example exploring super-radiant decay, illustrating that ACE can handle Hilbert spaces with higher-dimensional systems. Supplementary Section 6 further contains an example of the simulations of dispersive system–environment couplings as well as time-dependent driving and non-Hamiltonian loss terms acting directly on the environment. We have shown that ACE reproduces the exact results in limiting cases, and can interpolate between infinite and short memory scenarios within the same algorithm. In particular, it fully accounts for non-Markovian effects, system–environment correlations and non-Gaussian baths.

A fundamental restriction of ACE is that the environment must decompose into a set of separate modes without interactions between these modes. However, most typical models of open-system environments satisfy this requirement. Moreover, a recent study[54] adapting a method described elsewhere[55] has shown that one can extend tensor network methods to models where bath modes have nearest-neighbour interactions. Some environments have particular features that enable more specialized methods to be used, and these can be more efficient than the general method (ACE). For example, Gaussian baths with a broad continuum of modes have short memory times at high temperatures, and then iQUAPI[19] is extremely efficient. In contrast, for environments consisting of only a few discrete modes, ACE outperforms methods based on Gaussian path integrals (Supplementary Section 3). For spectral densities with several peaks on top of a broad background, the construction of a PT for Gaussian environments[36] can be readily combined with ACE to enable a hybrid approach within the common PT framework.

However, the unique feature of ACE is its generality. It can be used in situations where no specialized methods are available, and no additional derivations or modifications of the algorithm are required when a different system or environment is considered. As it fully accounts for all the environment influences, ACE can serve as a benchmark for approximate methods that may provide a more tangible interpretation of physical processes, or serve as a 'turnkey solution' to simulate concrete experiments. These features make ACE a valuable general-purpose tool for open quantum systems.

Online content

Any methods, additional references, Nature Research reporting summaries, source data, extended data, supplementary information, acknowledgements, peer review information; details of author contributions and competing interests; and statements of data and code availability are available at https://doi.org/10.1038/s41567-022-01544-9.

Received: 14 January 2021; Accepted: 9 February 2022;
Published online: 24 March 2022

References

1. Breuer, H.-P. and Petruccione, F. *The Theory of Open Quantum Systems* (Oxford Univ. Press, 2002).
2. Plenio, M. B. & Huelga, S. F. Dephasing-assisted transport: quantum networks and biomolecules. *New J. Phys.* **10**, 113019 (2008).
3. Rebentrost, P., Mohseni, M., Kassal, I., Lloyd, S. & Aspuru-Guzik, A. Environment-assisted quantum transport. *New J. Phys.* **11**, 033003 (2009).
4. Chin, A. W., Datta, A., Caruso, F., Huelga, S. F. & Plenio, M. B. Noise-assisted energy transfer in quantum networks and light-harvesting complexes. *New J. Phys.* **12**, 065002 (2010).
5. Beige, A., Braun, D., Tregenna, B. & Knight, P. L. Quantum computing using dissipation to remain in a decoherence-free subspace. *Phys. Rev. Lett.* **85**, 1762 (2000).
6. Verstraete, F., Wolf, M. M. & Cirac, J. I. Quantum computation and quantum-state engineering driven by dissipation. *Nat. Phys.* **5**, 633–636 (2009).
7. de Vega, I. & Alonso, D. Dynamics of non-Markovian open quantum systems. *Rev. Mod. Phys.* **89**, 015001 (2017).
8. Tanimura, Y. Stochastic Liouville, Langevin, Fokker–Planck, and master equation approaches to quantum dissipative systems. *J. Phys. Soc. Jpn* **75**, 082001 (2006).
9. Plenio, M. B. & Knight, P. L. The quantum-jump approach to dissipative dynamics in quantum optics. *Rev. Mod. Phys.* **70**, 101 (1998).
10. Redfield, A. G. The theory of relaxation processes. in *Advances in Magnetic Resonance, Advances in Magnetic and Optical Resonance* Vol. 1 (ed Waugh, J. S.) 1–32 (Academic Press, 1965).
11. Nazir, A. & McCutcheon, D. P. S. Modelling exciton–phonon interactions in optically driven quantum dots. *J. Phys.: Condens. Matter* **28**, 103002 (2016).
12. Breuer, H.-P., Laine, E.-M., Piilo, J. & Vacchini, B. Colloquium: non-Markovian dynamics in open quantum systems. *Rev. Mod. Phys.* **88**, 021002 (2016).
13. Tanimura, Y. & Kubo, R. Time evolution of a quantum system in contact with a nearly Gaussian-Markoffian noise bath. *J. Phys. Soc. Jpn* **58**, 101–114 (1989).
14. Tanimura, Y. Numerically 'exact' approach to open quantum dynamics: the hierarchical equations of motion (HEOM). *J. Chem. Phys.* **153**, 020901 (2020).
15. Prior, J., Chin, A. W., Huelga, S. F. & Plenio, M. B. Efficient simulation of strong system-environment interactions. *Phys. Rev. Lett.* **105**, 050404 (2010).
16. Somoza, A. D., Marty, O., Lim, J., Huelga, S. F. & Plenio, M. B. Dissipation-assisted matrix product factorization. *Phys. Rev. Lett.* **123**, 100502 (2019).
17. Nüßeler, A., Dhand, I., Huelga, S. F. & Plenio, M. B. Efficient simulation of open quantum systems coupled to a fermionic bath. *Phys. Rev. B* **101**, 155134 (2020).
18. Feynman, R. & Vernon, F. The theory of a general quantum system interacting with a linear dissipative system. *Ann. Phys.* **24**, 118 (1963).
19. Makri, N. & Makarov, D. E. Tensor propagator for iterative quantum time evolution of reduced density matrices. I. Theory. *J. Chem. Phys.* **102**, 4600 (1995).
20. Makri, N. & Makarov, D. E. Tensor propagator for iterative quantum time evolution of reduced density matrices. II. Numerical methodology. *J. Chem. Phys.* **102**, 4611 (1995).
21. Cygorek, M., Barth, A. M., Ungar, F., Vagov, A. & Axt, V. M. Nonlinear cavity feeding and unconventional photon statistics in solid-state cavity QED revealed by many-level real-time path-integral calculations. *Phys. Rev. B* **96**, 201201 (2017).
22. Strathearn, A., Kirton, P., Kilda, D., Keeling, J. & Lovett, B. W. Efficient non-Markovian quantum dynamics using time-evolving matrix product operators. *Nat. Commun.* **9**, 3322 (2018).
23. Cosacchi, M. et al. Path-integral approach for nonequilibrium multitime correlation functions of open quantum systems coupled to Markovian and non-Markovian environments. *Phys. Rev. B* **98**, 125302 (2018).
24. Denning, E. V., Bundgaard-Nielsen, M. & Mørk, J. Optical signatures of electron-phonon decoupling due to strong light-matter interactions. *Phys. Rev. B* **102**, 235303 (2020).
25. Cosacchi, M., Ungar, F., Cygorek, M., Vagov, A. & Axt, V. M. Emission-frequency separated high quality single-photon sources enabled by phonons. *Phys. Rev. Lett.* **123**, 017403 (2019).
26. Seidelmann, T. et al. Phonon-induced enhancement of photon entanglement in quantum dot-cavity systems. *Phys. Rev. Lett.* **123**, 137401 (2019).
27. Kaestle, O., Finsterhoelzl, R., Knorr, A. & Carmele, A. Continuous and time-discrete non-Markovian system-reservoir interactions: Dissipative coherent quantum feedback in Liouville space. *Phys. Rev. Research* **3**, 023168 (2021).
28. Vagov, A., Croitoru, M. D., Glässl, M., Axt, V. M. & Kuhn, T. Real-time path integrals for quantum dots: quantum dissipative dynamics with superohmic environment coupling. *Phys. Rev. B* **83**, 094303 (2011).

29. Quilter, J. H. et al. Phonon-assisted population inversion of a single InGaAs/GaAs quantum dot by pulsed laser excitation. *Phys. Rev. Lett.* **114**, 137401 (2015).
30. Koong, Z. X. et al. Coherent dynamics in quantum emitters under dichromatic excitation. *Phys. Rev. Lett.* **126**, 047403 (2021).
31. Palm, T. & Nalbach, P. Quasi-adiabatic path integral approach for quantum systems under the influence of multiple non-commuting fluctuations. *J. Chem. Phys.* **149**, 214103 (2018).
32. Simine, L. & Segal, D. Path-integral simulations with fermionic and bosonic reservoirs: transport and dissipation in molecular electronic junctions. *J. Chem. Phys.* **138**, 214111 (2013).
33. Rossi, F. & Kuhn, T. Theory of ultrafast phenomena in photoexcited semiconductors. *Rev. Mod. Phys.* **74**, 895 (2002).
34. Hsieh, C.-Y. & Cao, J. A unified stochastic formulation of dissipative quantum dynamics. I. Generalized hierarchical equations. *J. Chem. Phys.* **148**, 014103 (2018).
35. Hsieh, C.-Y. & Cao, J. A unified stochastic formulation of dissipative quantum dynamics. II. Beyond linear response of spin baths. *J. Chem. Phys.* **148**, 014104 (2018).
36. Jørgensen, M. R. & Pollock, F. A. Exploiting the causal tensor network structure of quantum processes to efficiently simulate non-Markovian path integrals. *Phys. Rev. Lett.* **123**, 240602 (2019).
37. Pollock, F. A., Rodríguez-Rosario, C., Frauenheim, T., Paternostro, M. & Modi, K. Non-Markovian quantum processes: complete framework and efficient characterization. *Phys. Rev. A* **97**, 012127 (2018).
38. Schollwöck, U. The density-matrix renormalization group in the age of matrix product states. *Ann. Phys.* **326**, 96 (2011).
39. Orús, R. A practical introduction to tensor networks: matrix product states and projected entangled pair states. *Ann. Phys.* **349**, 117 (2014).
40. Luchnikov, I. A., Vintskevich, S. V., Ouerdane, H. & Filippov, S. N. Simulation complexity of open quantum dynamics: connection with tensor networks. *Phys. Rev. Lett.* **122**, 160401 (2019).
41. Brandes, T. & Kramer, B. Spontaneous emission of phonons by coupled quantum dots. *Phys. Rev. Lett.* **83**, 3021 (1999).
42. Barth, A. M., Vagov, A. & Axt, V. M. Path-integral description of combined Hamiltonian and non-Hamiltonian dynamics in quantum dissipative systems. *Phys. Rev. B* **94**, 125439 (2016).
43. Nagy, D., Szirmai, G. & Domokos, P. Critical exponent of a quantum-noise-driven phase transition: the open-system Dicke model. *Phys. Rev. A* **84**, 043637 (2011).
44. Mitchison, M. T. & Plenio, M. B. Non-additive dissipation in open quantum networks out of equilibrium. *New J. Phys.* **20**, 033005 (2018).
45. Maguire, H., Iles-Smith, J. & Nazir, A. Environmental nonadditivity and Franck-Condon physics in nonequilibrium quantum systems. *Phys. Rev. Lett.* **123**, 093601 (2019).
46. Gribben, D. et al. Exact dynamics of nonadditive environments in non-Markovian open quantum systems. *PRX Quantum* **3**, 010321 (2022).
47. Krummheuer, B., Axt, V. M., Kuhn, T., D'Amico, I. & Rossi, F. Pure dephasing and phonon dynamics in GaAs- and GaN-based quantum dot structures: interplay between material parameters and geometry. *Phys. Rev. B* **71**, 235329 (2005).
48. Roy-Choudhury, K. & Hughes, S. Spontaneous emission from a quantum dot in a structured photonic reservoir: phonon-mediated breakdown of Fermi's golden rule. *Optica* **2**, 434–437 (2015).
49. Hoeppe, U. et al. Direct observation of non-Markovian radiation dynamics in 3D bulk photonic crystals. *Phys. Rev. Lett.* **108**, 043603 (2012).
50. Gangloff, D. A. et al. Quantum interface of an electron and a nuclear ensemble. *Science* **364**, 62–66 (2019).
51. Scheuer, J. et al. Robust techniques for polarization and detection of nuclear spin ensembles. *Phys. Rev. B* **96**, 174436 (2017).
52. Wang, H. & Thoss, M. Quantum dynamical simulation of electron-transfer reactions in an anharmonic environment. *J. Phys. Chem. A* **111**, 10369 (2007).
53. Bramberger, M. & De Vega, I. Dephasing dynamics of an impurity coupled to an anharmonic environment. *Phys. Rev. A* **101**, 012101 (2020).
54. Ye, E. & Chan, G. K.-L. Constructing tensor network influence functionals for general quantum dynamics. *J. Chem. Phys.* **155**, 044104 (2021).
55. Bañuls, M. C., Hastings, M. B., Verstraete, F. & Cirac, J. I. Matrix product states for dynamical simulation of infinite chains. *Phys. Rev. Lett.* **102**, 240603 (2009).

Methods

Derivation of PT. We consider an arbitrary open quantum system specified by the Hamiltonian $H=H_S+H_E$, where H_S is the free-system Hamiltonian without coupling to the environment. For simplicity of notation, we assume a time-independent Hamiltonian in the following, but generalization to the time-dependent case is straightforward. The time evolution of the system density operator $\hat{\rho}_S$ can be obtained from the time evolution operator $U(t)$ of the total system, including the environment, by tracing out the environment to give

$$\hat{\rho}_S(t) = \mathrm{Tr}_E\left[U(t)\,(\hat{\rho}_S(0)\otimes\hat{\rho}_E(0))\,U^\dagger(t)\right]. \tag{13}$$

We discretize the time evolution operator $U(t)=\prod_{l=1}^{n}U(\Delta t)$ on a time grid $t_l=l\Delta t$, where $l=1\ldots n$, and apply a Trotter decomposition $U(\Delta t)=\mathrm{e}^{-\frac{i}{\hbar}H_E\Delta t}\,\mathrm{e}^{-\frac{i}{\hbar}H_S\Delta t}+\mathcal{O}(\Delta t^2)$. Next, we introduce a complete basis for the system (ν or μ) as well as for the full environment (ξ or η). We then introduce the matrix elements

$$A^{\nu_l\tilde{\nu}_l}_{\xi_l\xi_{l-1}} = \langle\nu_l,\xi_l|\,\mathrm{e}^{-\frac{i}{\hbar}H_E\Delta t}\,|\tilde{\nu}_l,\xi_{l-1}\rangle, \tag{14}$$

$$M^{\tilde{\nu}_l\nu_{l-1}} = \langle\tilde{\nu}_l|\,\mathrm{e}^{-\frac{i}{\hbar}H_S\Delta t}\,|\nu_{l-1}\rangle. \tag{15}$$

By using calligraphic symbols, their counterparts in Liouville space can be expressed as

$$\mathcal{A}^{(\nu_l,\mu_l),(\tilde{\nu}_l,\tilde{\mu}_l)}_{(\xi_l,\eta_l),(\xi_{l-1},\eta_{l-1})} := A^{\nu_l\tilde{\nu}_l}_{\xi_l\xi_{l-1}}A^{\mu_l\tilde{\mu}_l*}_{\eta_l\eta_{l-1}}, \tag{16}$$

$$\mathcal{M}^{\tilde{\nu}_l\nu_{l-1}}_{\tilde{\mu}_l\mu_{l-1}} := M^{\tilde{\nu}_l\nu_{l-1}}M^{\tilde{\mu}_l\mu_{l-1}*}. \tag{17}$$

The reduced system density matrix at time step $t_n=n\Delta t$ can then be expressed as

$$\rho_{\nu_n\mu_n} = \sum_{\substack{\nu_{n-1}\cdots\nu_0\\ \tilde{\nu}_n\cdots\tilde{\nu}_1}}\sum_{\substack{\mu_{n-1}\cdots\mu_0\\ \tilde{\mu}_n\cdots\tilde{\mu}_1}} I^{(\nu_n\tilde{\nu}_n)\ldots(\nu_1\tilde{\nu}_1)}_{(\mu_n\tilde{\mu}_n)\ldots(\mu_1\tilde{\mu}_1)}\left(\prod_{l=1}^{n}\mathcal{M}^{\tilde{\nu}_l\nu_{l-1}}_{\tilde{\mu}_l\mu_{l-1}}\right)\rho_{\nu_0\mu_0}, \tag{18}$$

where

$$I^{(\nu_n\tilde{\nu}_n)\ldots(\nu_1\tilde{\nu}_1)}_{(\mu_n\tilde{\mu}_n)\ldots(\mu_1\tilde{\mu}_1)} = \sum_{\substack{\xi_n\cdots\xi_0\\ \eta_n\cdots\eta_0}}\delta_{\xi_n\eta_n}\left(\prod_{l=1}^{n}\mathcal{A}^{(\nu_l,\mu_l),(\tilde{\nu}_l,\tilde{\mu}_l)}_{(\xi_l,\eta_l),(\xi_{l-1},\eta_{l-1})}\right)\rho^E_{\xi_0\eta_0}. \tag{19}$$

Here $\rho_{\nu_0\mu_0}$ and $\rho^E_{\xi_0\eta_0}$ are the initial system and environment states, respectively. The implicit assumption of a factorization of the initial state into the system and environment parts, that is, uncorrelated initial states, does not restrict the generality, because the initial states with finite system–environment correlations can always be rewritten as sums of the product states using the Schmidt decomposition.

By combining pairs of Hilbert space indices into Liouville space indices, namely, $\alpha_l=(\nu_l,\mu_l)$, $\tilde{\alpha}_l=(\tilde{\nu}_l,\tilde{\mu}_l)$ and $d_l=(\xi_l,\eta_l)$, equation (18) becomes equation (1) and equation (19) takes the form of equation (2). The matrices $\mathcal{Q}$ can be obtained by comparing with equation (19) as

$$\mathcal{Q}^{(\alpha_l,\tilde{\alpha}_l)}_{d_ld_{l-1}} = \begin{cases}\delta_{d_0,1}\sum_{d_0'}\mathcal{A}^{\alpha_1,\tilde{\alpha}_1}_{d_1,d_0'}\rho^E_{d_0'} & l=1,\\ \mathcal{A}^{\alpha_l,\tilde{\alpha}_l}_{d_l,d_{l-1}} & 1<l<n,\\ \delta_{d_n,1}\sum_{d_n'}\mathfrak{I}_{d_n'}\mathcal{A}^{\alpha_n,\tilde{\alpha}_n}_{d_n',d_{n-1}} & l=n.\end{cases} \tag{20}$$

where $\mathfrak{I}_{d_n'=(\xi_n,\eta_n)}=\delta_{\xi_n,\eta_n}$.

Network summation. The network structure determining the reduced system density matrix (Fig. 1d) can be most easily evaluated by propagating the quantity $\mathcal{R}_{\alpha_ld_l}$ defined recursively via

$$\mathcal{R}_{\alpha_0 1} = \rho_{\alpha_0} = \rho_{\nu_0\mu_0}, \tag{21a}$$

$$\mathcal{R}_{\alpha_ld_l} = \sum_{\tilde{\alpha}_l\alpha_{l-1}}\sum_{d_{l-1}}\mathcal{Q}^{(\alpha_l,\tilde{\alpha}_l)}_{d_ld_{l-1}}\mathcal{M}^{\tilde{\alpha}_l\alpha_{l-1}}\mathcal{R}_{\alpha_{l-1}d_{l-1}}. \tag{21b}$$

Comparing equations (1) and (2), it can be seen that the density matrix at the last time step is given by $\rho_{\alpha_n}=\mathcal{R}_{\alpha_n 1}$.

When the environment time evolution operator is unitary, the reduced density matrix ρ_{α_l} at intermediate time steps t_l can be easily obtained from $\mathcal{R}_{\alpha_ld_l}$ as

$$\rho_{\alpha_l} = \sum_{d_l} q_{d_l}\mathcal{R}_{\alpha_ld_l} \tag{22}$$

using the closures q_{d_l} defined by the recursion (Supplementary Section 1 provides a detailed derivation)

$$q_{d_n=1} = 1, \tag{23}$$

$$q_{d_{l-1}} = \sum_{d_l} q_{d_l}\sum_{\alpha_l}\mathfrak{I}_{\alpha_l}\mathcal{Q}^{(\alpha_l 0)}_{d_ld_{l-1}}. \tag{24}$$

Thus, in practice, one needs to calculate only a single PT MPO with n time steps, where $n\Delta t=t_{\mathrm{final}}$ is the final time of interest, and yields the density matrix at all intermediate time steps $l\Delta t$ at marginal numerical extra cost.

PT combination rule. To combine the influences of multiple environments or of independent environments into a single PT, we consider a system coupled to multiple environmental degrees of freedom (which we henceforth call modes) via

$$H_E = \sum_{k=1}^{N_E}H_E^k. \tag{25}$$

We define the partial sum of the Hamiltonians from modes $1,2,\ldots K$ as

$$H_E[K] = \sum_{k=1}^{K}H_E^k \tag{26}$$

and $\mathcal{Q}^{(\alpha_l,\tilde{\alpha}_l)}_{d_ld_{l-1}}[K]$ denotes the lth MPO matrix of the PT including the influences of the modes $1,2,\ldots K$. Then, by means of the symmetric Trotter decomposition

$$\begin{aligned}\mathrm{e}^{-\frac{i}{\hbar}H_E[K]\Delta t} &= \mathrm{e}^{-\frac{i}{\hbar}\left(H_E[K-1]+H_E^K\right)\Delta t}\\ &= \mathrm{e}^{-\frac{i}{\hbar}H_E^K\frac{\Delta t}{2}}\mathrm{e}^{-\frac{i}{\hbar}H_E[K-1]\Delta t}\mathrm{e}^{-\frac{i}{\hbar}H_E^K\frac{\Delta t}{2}}+O(\Delta t^3),\end{aligned} \tag{27}$$

the influence of mode K can be combined with the PT already containing the influences of the first $K-1$ modes by

$$\begin{aligned}&\mathcal{Q}^{(\alpha_l,\tilde{\alpha}_l)}_{(d_l',d_l)(d_{l-1}',d_{l-1})}[K]\\ &\approx\sum_{\gamma_l,\tilde{\gamma}_l,\tilde{d}_l}\mathcal{B}^{(\alpha_l,\gamma_l)}_{d_l\tilde{d}_l}(K)\;\mathcal{Q}^{(\gamma_l,\tilde{\gamma}_l)}_{d_l'd_{l-1}'}[K-1]\;\mathcal{B}^{(\tilde{\gamma}_l,\tilde{\alpha}_l)}_{\tilde{d}_ld_{l-1}}(K),\end{aligned} \tag{28}$$

where

$$\begin{aligned}&\mathcal{B}^{((\nu_l,\mu_l),(\tilde{\nu}_l,\tilde{\mu}_l))}_{(\xi_l,\eta_l),(\xi_{l-1},\eta_{l-1})}(K)\\ &=\langle\nu_l,\xi_l|\,\mathrm{e}^{-\frac{i}{\hbar}H_E^K\frac{\Delta t}{2}}\,|\tilde{\nu}_l,\xi_{l-1}\rangle\,\langle\tilde{\mu}_l,\eta_{l-1}|\,\mathrm{e}^{\frac{i}{\hbar}H_E^K\frac{\Delta t}{2}}\,|\mu_l,\eta_l\rangle.\end{aligned} \tag{29}$$

This step is visualized in Fig. 1e.

In practice, we start with the trivial PT MPO with matrices $\mathcal{Q}^{(\alpha_l,\tilde{\alpha}_l)}_{d_ld_{l-1}}[0]=\delta_{d_l,1}\delta_{d_{l-1},1}\delta_{\alpha_l,\tilde{\alpha}_l}$ and add the influence of all the environment modes by recursively applying equation (28) until $K=N_E$. After each combination step, the PT MPO is compressed using the SVD-based compression as described in the next section.

MPO compression. To reduce the inner dimension of the MPO representing the PT, we perform SVD sweeps across the MPO chain. Any matrix $A\in\mathbb{C}^{n\times m}$ can be factorized into a product

$$A = U\Sigma V^\dagger, \tag{30}$$

where $U\in\mathbb{C}^{n\times k}$ and $V\in\mathbb{C}^{m\times k}$ are matrices with orthogonal column vectors and Σ is a diagonal matrix containing the $k=\min(n,m)$ real and non-negative singular values σ_i in descending order. Here we start with the first MPO matrix and define

$$A_{d_1,(\alpha_1,\tilde{\alpha}_1)} = \mathcal{Q}^{(\alpha_1,\tilde{\alpha}_1)}_{d_11}. \tag{31}$$

We calculate the SVD of matrix A. To reduce the inner dimension, we truncate the matrices U,Σ and V, keeping only the $k_{\mathrm{eff}}\le k$ singular values with $\sigma_i>\epsilon\sigma_1$, where σ_1 is the largest singular value of A and ϵ is a predefined threshold. Then, we replace $\mathcal{Q}^{(\alpha_1,\tilde{\alpha}_1)}_{d_11}$ by $\left(V^\dagger\right)_{k_{\mathrm{eff}}(\alpha_1,\tilde{\alpha}_1)}$ and multiply the next matrix $\mathcal{Q}^{(\alpha_2,\tilde{\alpha}_2)}_{d_2d_1}$ from the right by $U_{d_1k_{\mathrm{eff}}}\sigma_{k_{\mathrm{eff}}}$ and perform the SVD of

$$A_{d_2,(\alpha_2,\tilde{\alpha}_2,k_{\mathrm{eff}})} = \sum_{d_1}\mathcal{Q}^{(\alpha_2,\tilde{\alpha}_2)}_{d_2d_1}U_{d_1k_{\mathrm{eff}}}\sigma_{k_{\mathrm{eff}}}. \tag{32}$$

The reduction is continued until the end of the MPO is reached. Then, another line sweep is performed in the opposite direction. Note that sweeps along the whole chain are required between each PT combination step, because information necessary to effectively compress the MPO, such as the initial environment state, needs to be propagated from the ends throughout the MPO.

In the overall process, the inner dimensions d_i are reduced to the respective effective ranks k_{eff}, where the latter are controlled by threshold ϵ.

Parameters for QD, QD–phonon and QD–photon Hamiltonians. The effects of the dot–phonon coupling are completely defined by the phonon spectral density

$$J(\omega) = \sum_{\mathbf{q}} \gamma_{\mathbf{q}}^2 \delta(\omega - \omega_{\mathbf{q}}). \tag{33}$$

Using established parameters[47] for a GaAs QD with electron radius $a_e = 3.0\,\mathrm{nm}$ and hole radius $a_h = a_e/1.15$,

$$J(\omega) = \frac{\omega^3}{4\pi^2\rho\hbar c_s^5}\left(D_e e^{-\omega^2 a_e^2/(4c_s^2)} - D_h e^{-\omega^2 a_h^2/(4c_s^2)}\right)^2 \tag{34}$$

with mass density $\rho = 5{,}370\,\mathrm{kg\,m^{-3}}$; speed of sound $c_s = 5{,}110\,\mathrm{m\,s^{-1}}$; and electron and hole deformation potential constants $D_e = 7.0\,\mathrm{eV}$ and $D_h = -3.5\,\mathrm{eV}$, respectively. We discretize the phonon continuum using steps of equal width so that $\omega_q = q\mathrm{d}\omega$ with $\mathrm{d}\omega = \omega_{\max}/N_E$, $N_E = 100$ and $\omega_{\max} = 5\,\mathrm{meV}/\hbar$ and we obtain the couplings γ_q from the phonon density of states using $\gamma_q = \sqrt{J(\omega_q)\mathrm{d}\omega}$. The phonon modes are initially assumed to be in thermal equilibrium with temperature $T = 4\,\mathrm{K}$. We have checked that for these parameters, it is enough to consider up to two excitations per mode.

We use a radiative decay rate of $\kappa = 0.1\,\mathrm{ps^{-1}}$. When the electromagnetic environment is microscopically treated, we assume a constant density of states with bandwidth $\omega_{\mathrm{BW}} = 10\,\mathrm{ps^{-1}}$, discretized using $N_E = 100$ equally spaced modes. The coupling constants g_k are taken to be constant, and the value is chosen such that Fermi's golden rule reproduces the radiative decay rate κ. The PTs for the phonon and photon environments are separately calculated and combined using equation (28) without performing a final SVD sweep. For both baths, we use time steps $\Delta t = 0.1\,\mathrm{ps}$ and an MPO compression threshold $\epsilon = 5 \times 10^{-8}$.

The Gaussian excitation pulse is detuned by $\hbar\delta = 1.5\,\mathrm{meV}$ above the QD resonance and the envelope is described by

$$\Omega(t) = \frac{A}{\sqrt{2\pi}\sigma}\exp\left(-\frac{(t-t_0)^2}{2\sigma^2}\right), \tag{35}$$

where we use the pulse area $A = 3\pi$, pulse centre $t_0 = 7\,\mathrm{ps}$, $\sigma = \tau_{\mathrm{FWHM}}/\left(2\sqrt{2\ln 2}\right)$ and $\tau_{\mathrm{FWHM}} = 5\,\mathrm{ps}$.

Numerical implementation. We have implemented ACE in a C++98 code using the Eigen library to calculate the matrix exponentials and SVDs. All the calculations have been performed on a conventional laptop computer with Intel Core i5-8265U processor and 16 GB random-access memory. The computation times for the presented examples are listed in Supplementary Section 3.

Data availability

The data presented in the figures including the parameter files to generate them are available online in the 'examples' subdirectory of the Zenodo repository at https://doi.org/10.5281/zenodo.5214128.

Code availability

The C++ computer code including documentation is available online at https://doi.org/10.5281/zenodo.5214128.

Acknowledgements

M. Cosacchi and V.M.A. are grateful for funding by the Deutsche Forschungsgemeinschaft (DFG, German Research Foundation) under project no. 419036043. A.V. acknowledges support from the Russian Science Foundation under Project 18-12-00429 and from the Basic Research Program at the HSE University. M. Cygorek and E.M.G. acknowledge funding from EPSRC grant no. EP/T01377X/1. B.W.L. and J.K. were supported by EPSRC grant no. EP/T014032/1.

Author contributions

M. Cygorek, M. Cosacchi, A.V., and V.M.A. developed the concept of explicitly constructing the PT to simulate open quantum systems with arbitrary system–environment couplings. M. Cygorek, B.W.L., J.K. and E.M.G. contributed the idea of using MPO representations for efficient storage and evaluation of the PT. M. Cygorek is responsible for the details of the algorithm, implementation in the form of C++ code and generation of data. All the authors analysed and discussed the results and contributed to writing the Article.

Competing interests

The authors declare no competing interests.

Additional information

Supplementary information The online version contains supplementary material available at https://doi.org/10.1038/s41567-022-01544-9.

Correspondence and requests for materials should be addressed to Moritz Cygorek or Erik M. Gauger.

Peer review information *Nature Physics* thanks the anonymous reviewers for their contribution to the peer review of this work.